

# Fluorine and chlorine in mantle minerals and the halogen budget of the Earth's mantle

B. M. Urann<sup>1</sup> · V. Le Roux<sup>1</sup> · K. Hammond<sup>1</sup> · H. R. Marschall<sup>1,2</sup> · C.-T. A. Lee<sup>3</sup> · B. D. Monteleone<sup>1</sup>

Received: 10 January 2017 / Accepted: 8 May 2017  
© Springer-Verlag Berlin Heidelberg 2017

**Abstract** The fluorine (F) and chlorine (Cl) contents of arc magmas have been used to track the composition of subducted components, and the F and Cl contents of MORB have been used to estimate the halogen content of depleted MORB mantle (DMM). Yet, the F and Cl budget of the Earth's upper mantle and their distribution in peridotite minerals remain to be constrained. Here, we developed a method to measure low concentrations of halogens ( $\geq 0.4 \mu\text{g/g}$  F and  $\geq 0.3 \mu\text{g/g}$  Cl) in minerals by secondary ion mass spectroscopy. We present a comprehensive study of F and Cl in co-existing natural olivine, orthopyroxene, clinopyroxene, and amphibole in seventeen samples from different tectonic settings. We support the hypothesis that F in olivine is controlled by melt polymerization, and that F in pyroxene is controlled by their Na and Al contents, with some effect of melt polymerization. We infer that Cl compatibility ranks as follows: amphibole > clinopyroxene > olivine ~ orthopyroxene, while F compatibility ranks as follows: amphibole > clinopyroxene > orthopyroxene  $\geq$  olivine, depending on the tectonic context. In

addition, we show that F, Cl, Be and B are correlated in pyroxenes and amphibole. F and Cl variations suggest that interaction with slab melts and fluids can significantly alter the halogen content of mantle minerals. In particular, F in oceanic peridotites is mostly hosted in pyroxenes, and proportionally increases in olivine in subduction-related peridotites. The mantle wedge is likely enriched in F compared to un-metasomatized mantle, while Cl is always low ( $< 1 \mu\text{g/g}$ ) in all tectonic settings studied here. The bulk anhydrous peridotite mantle contains 1.4–31  $\mu\text{g/g}$  F and 0.14–0.38  $\mu\text{g/g}$  Cl. The bulk F content of oceanic-like peridotites (2.1–9.4  $\mu\text{g/g}$ ) is lower than DMM estimates, consistent with F-rich eclogite in the source of MORB. Furthermore, the bulk Cl budget of all anhydrous peridotites studied here is lower than previous DMM estimates. Our results indicate that nearly all MORB may be somewhat contaminated by seawater-rich material and that the Cl content of DMM could be overestimated. With this study, we demonstrate that the halogen contents of natural peridotite minerals are a unique tool to understand the cycling of halogens, from ridge settings to subduction zones.

Communicated by Timothy L. Grove.

**Electronic supplementary material** The online version of this article (doi:10.1007/s00410-017-1368-7) contains supplementary material, which is available to authorized users.

✉ B. M. Urann  
burann@whoi.edu

<sup>1</sup> Woods Hole Oceanographic Institution, 266 Woods Hole Road, Woods Hole, MA 02543, USA

<sup>2</sup> Goethe Universität Frankfurt, Institut für Geowissenschaften, Altenhöferallee 1, 60438 Frankfurt am Main, Germany

<sup>3</sup> Department of Earth Science, Rice University, MS-126, 6100 Main St., Houston, TX 77005, USA

**Keywords** Fluorine and chlorine content of mantle minerals · Halogen partitioning · Halogen budget of DMM · Peridotite

## Introduction

Fluorine (F) and chlorine (Cl) concentrations in arc-derived melts have been used to track the composition of subducted components transported from the slab to the hot corner of the mantle wedge (Straub and Layne 2003; Dalou et al. 2014; Le Voyer et al. 2015; Van den Bleeken and Koga 2015), and the F and Cl contents of MORB have been used

to estimate the halogen content of the depleted MORB mantle (Michael and Schilling 1989; Saal et al. 2002; Salters and Stracke 2004; Shaw et al. 2010; Shimizu et al. 2016). Unlike H<sub>2</sub>O or CO<sub>2</sub>, the F and Cl content of mantle melts do not vary significantly during their ascent to the surface, as they only degas at shallow pressures (<20 and 100 MPa, respectively; (Spilliaert et al. 2006). Thus, the F and Cl contents of primitive mantle melts should reflect the halogen content of the mantle source at the time of magma genesis. Studies of arc melt inclusions have shown that incompatible elements F and Cl are enriched in arc magmas relative to MORB. F concentrations are 1–16 times higher in arcs than in N-MORB (Le Voyer et al. 2010; Wu and Koga 2013). It has been suggested that F transport from the subducted slab to the overlying mantle wedge must be achieved by percolation of silicate melts (Wu and Koga 2013), as F solubility in silicate melts is high (e.g., Dingwell 1989), and increases with increasing H<sub>2</sub>O content dissolved in the melt (Dalou et al. 2014; Dalou and Mysen 2015). Similarly, Cl concentrations may be up to 20 times higher in arcs than in N-MORB (Jenner and O'Neill 2012; Dalou et al. 2014) because Cl is highly soluble in slab aqueous fluids (e.g., Brennan 1994) and effectively lost from the slab during subduction process (Philippot et al. 1998; Straub and Layne 2003; Scambelluri et al. 2004; Bonifacie et al. 2008; Marschall et al. 2009; John et al. 2011). During subduction, Cl may be directly added to the mantle wedge via fluids or fluid-rich rocks. However, although Cl/F of seawater is 15,000–20,000, the Cl/F ratio of aqueous fluids in arcs is usually <10, depending on the location of the arc (Straub and Layne 2003; Le Voyer et al. 2010). Thus, although previous studies suggest that F and Cl should be enriched in the mantle wedge compared to the depleted MORB mantle (DMM), the distribution of F and Cl in peridotite minerals from ridge and convergent settings, and their cycling throughout the subduction process, are yet to be determined (Debret et al. 2013).

Literature data for F and Cl in natural peridotite minerals are limited. Bénard et al. (2017), Debret et al. (2013) and Beyer et al. (2012) have reported a range of 2–33, 4–17, and 14–20 µg/g Cl for olivine (Ol), orthopyroxene (Opx), and clinopyroxene (Cpx), respectively. Previous studies on F in natural peridotite minerals (Peslier and Luhr 2006; Bromiley and Kohn 2007; Beyer et al. 2012; Guggino 2012; Guggino and Hervig 2012; Fabbrizio et al. 2013; Mosenfelder and Rossman 2013a, b; Debret et al. 2013; Warren and Hauri 2014; Bénard et al. 2017) have suggested that olivine, orthopyroxene and clinopyroxene contain non negligible amounts of F (1–51, <1–41, and 8–46 µg/g, respectively), most likely incorporated into oxygen sites. In particular, Mosenfelder and Rossman (2013b) have proposed that F<sup>-</sup> is incorporated into clinopyroxenes on the oxygen site; charge balanced by substitution of Si<sup>4+</sup> with

Al<sup>3+</sup> and/or Fe<sup>3+</sup> or coupled substitution with monovalent cations in the M2 site. These studies support the idea that olivine and pyroxene, the main constituents of the Earth's upper mantle, can accommodate most if not all of the F budget of the mantle (Beyer et al. 2012; Mosenfelder and Rossman 2013a), assuming that apatite is not stable in the asthenospheric source of MORB (Konzett and Frost 2009).

Here, we present the first extensive study of F and Cl in natural and coexisting mantle minerals olivine, orthopyroxene, and clinopyroxene, and amphibole. First, we describe the analytical developments that were required to measure low concentrations of halogens ( $\geq 0.4$  µg/g F and  $\geq 0.3$  µg/g Cl) in mantle minerals by secondary ion mass spectrometry (SIMS), and we present the recommended analytical settings used on the IMS 1280 hosted at the NENIMF facility (Woods Hole Oceanographic Institution, USA). Second, we present our results on the distribution of F and Cl in natural peridotite minerals and compare them to the limited literature available for natural peridotite minerals and experimental runs. Then, we discuss the incorporation mechanisms of F and Cl into mantle minerals and we identify the key parameters that control the abundances of F and Cl in mantle minerals. We also compare the F and Cl contents obtained in this study with Li, Be, and B values for pyroxene and amphibole from the Finero massif (Italy). Finally, we discuss the implications of this work for halogen cycling during subduction and the halogen budget of the peridotite mantle.

## Sample description

We selected a total of seventeen natural peridotite samples for study. Eleven olivine grains, seventeen orthopyroxene grains, fifteen clinopyroxene grains, and two amphibole grains were analyzed for F and Cl. In addition, one clinopyroxene grain, one orthopyroxene grain and one amphibole were profiled for Li, Be, and B. The samples were chosen to represent a variety of tectonic environments including supra-subduction ophiolites (Josephine Peridotite, USA), subduction-metasomatized subcontinental lithospheric mantle (Finero, Ivrea Zone, Italy), un-metasomatized subcontinental lithospheric mantle (Balmuccia, Ivrea Zone, Italy), metasomatized mantle-derived xenoliths (Colorado Plateau, USA), and fresh abyssal peridotites from the Mid Atlantic Ridge spreading center (MAR). Sample descriptions and mineral modes are available in Tables 1 and 5 in Electronic Supplementary Material, respectively. Below we provide a brief description of the geological contexts of our samples.

The Josephine Peridotite (USA) is a ~640 km<sup>2</sup> ultramafic massif located in southern Oregon and consists mostly of depleted harzburgites and lherzolites, with subordinate

dunites and pyroxenites. It is part of a supra-subduction ophiolite that was emplaced ~157 Ma ago. Previous studies have revealed that the compositional variability of the mantle occurs at two scales (Le Roux et al. 2014). Large compositional variations occur at kilometer scales and are consistent with a model where variable degrees of melt extraction (10 to >23%) occurred while the mantle was continuously re-supplied with small amounts (<0.1 wt%) of seawater-like fluids derived from the underlying subducting plate (Le Roux et al. 2014). Areas where fluid-rich materials were focused experienced significantly greater degrees of melting compared to a typical MORB mantle. Single outcrops display sharp compositional transitions attributed to local melt-rock reactions, where partial re-equilibration of harzburgites with boninite melts is recorded. Our samples feature harzburgites (J127-19, J127-17) and lherzolites (J98-10, J127-09) that reflect the km-scale compositional variations observed in the Josephine peridotite.

The Finero and Balmuccia Massifs (Italy) are part of the Ivrea Zone, a region of exposed lower crust and mantle peridotite tectonically emplaced after mantle metasomatism occurred during Triassic subduction. The Balmuccia Peridotite consists largely of lherzolites, with minor harzburgites (sample BM5) and dunites (Selverstone and Sharp 2011). The Balmuccia lherzolites underwent minor melt depletion (~5%), little to no enrichment, and thus are relatively pristine (Selverstone and Sharp 2011). The Finero Peridotite is compositionally more variable, and may have undergone substantial metasomatic enrichment from at least two metasomatic agents including a hydrated clinopyroxene component and an isotopically heavy component, enriched in LILE, HFSE and Cl (Selverstone and Sharp 2011). Finero samples (Fin10, Fin1b) contain abundant olivine, orthopyroxene, clinopyroxene, amphibole and phlogopite, and provide a unique opportunity to study the distribution of halogens and other volatile elements in coexisting hydrous and anhydrous phases.

Mantle-derived xenoliths presented in this study define a transect from the Basin and Range to the Colorado Plateau (USA) (Li et al. 2008). Samples were selected to include subcontinental lithospheric mantle samples thought to have undergone varying degrees of hydration/metasomatism from the subduction of the Farallon plate during the early Cenozoic (Dixon et al. 2004; Lee 2005; Humphreys and Niu 2009). Dish Hill lherzolites (DHS02;07;18) are from the Pliocene alkali basalt cinder cone in the Basin and Range (westernmost), and displayed equigranular to porphyroclastic textures (Luffi et al. 2009). Sample GC2b is a spinel harzburgite from the Grand Canyon Uinkaret volcanic field on the western edge of the Colorado Plateau (Li et al. 2008). San Carlos xenolith sample (SC-99) comes from a Pliocene alkali basalt lava flow in the Basin and Range province, south of the Colorado Plateau. Sample

KLB1, a lherzolite, was collected from ejecta deposits of the basanitic maar volcano that created Kilbourne Hole, at the southern edge of the Rio Grande Rift. Sample TH2, a spinel harzburgite, was recovered at the Thumb, an ultrapotassic minette diatreme of the Eocene Navajo Volcanic Field (Roden 1981; Lee 2005). Detailed sample descriptions can be found in Li et al. (2008).

MAR sample KNR210-05 D41-24 is a spinel harzburgite with a proto-granular texture and grain size ~1–5 mm. The sample was collected from the 16°30'N region of the Mid Atlantic Ridge, a region of slow spreading (S.R. 25 km/Ma) and active detachment faulting where abundant mantle peridotite is exposed on the seafloor, with limited axial volcanism (Smith et al. 2014). This region consists primarily of depleted/ultra-depleted harzburgite (Silantsev et al. 2016).

Nine samples were analyzed as thin sections (Josephine series, MAR, Fin1b, Fin10), and eight samples were mounted as individual grains in indium (KLB-1, SC99, GC2B, TH2, DHS2, DHS7, DHS18, BM5).

## Methods

All F and Cl measurements were conducted on a Cameca IMS 1280 at the Northeast National Ion Microprobe Facility (Woods Hole Oceanographic Institution). Details on sample preparation procedures and technical developments can be found in the Supplementary Material section. We utilized a primary Cs<sup>+</sup> beam of 5.0–7.5 nA to sputter through the sample surface. A 30 × 30 μm<sup>2</sup> raster and a 400-μm field aperture were used, which only allowed transmission of ions from the innermost 3.8 μm diameter of the beam crater. Secondary magnet mass calibration was done before each measurement, and mass resolving power was >6000 (m/Δm at 10% peak height). We measured <sup>19</sup>F/<sup>30</sup>Si and <sup>35</sup>Cl/<sup>30</sup>Si ratios in glass standards D51-3, D52-5, 519-4-1, 46D, 1649-3, 1654-3, to produce a calibration curve for each session. Glass standard F and Cl concentrations are available in Rose-Koga et al. (2008). Matrix effects were considered negligible, following the conclusions of Hauri et al. (2002). No nominally anhydrous mineral standards currently exist for F and Cl. However, the F and Cl contents of Herasil 102, an optical quality glass, and Synthetic Forsterite were measured in each of the six sessions over the course of 1 year (Fig. 1a, b) and are believed to be very low (E. Hauri, *pers. comm*). Herasil systematically displayed the lowest F contents and Synthetic Forsterite the lowest Cl contents. We conservatively assumed that Herasil contains no F and Synthetic Forsterite contains no Cl, such that measured F in Herasil and measured Cl in Synthetic Forsterite represent our maximum background values for

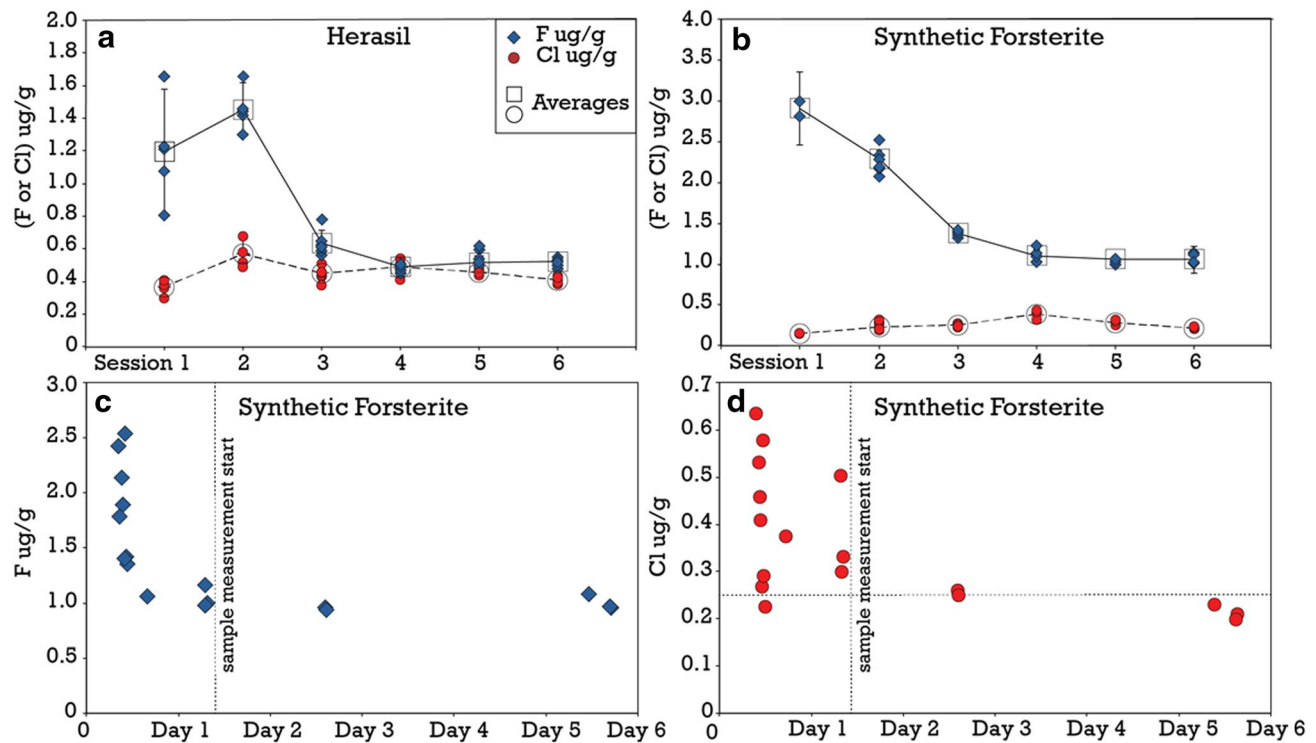


**Fig. 1** **a** F and Cl concentrations in Herasil glass over six analytical sessions, with 95% confidence standard error. **b** F and Cl concentrations in Synthetic Forsterite over six analytical sessions, with 95% confidence standard error. **c** F and **d** Cl concentrations in Synthetic Forsterite over a 6-day SIMS session showing the setting opti-

mization at the beginning of each session, after which natural samples measurements started (vertical line) once Synthetic Forsterite stabilized at its lowest F and Cl value (horizontal line shows the maximum Cl background value for that particular session). Session measurements can be found in Table 1 in Electronic Supplementary Material

F and Cl, respectively, for each session (Table 1 in Electronic Supplementary Material). This step was critical to conservatively estimate our errors, especially for very low F and Cl concentrations. The decrease of our background values from session 1 to session 4 (Fig. 1a, b) reflects the technical developments associated with this work. In Fig. 1c, d, we illustrate a typical week of measurements, where machine tuning is essential to reach the lowest possible background values. Analytical uncertainties over ten counting cycles (internal precision: typical standard error (SE) <1% F, <2% Cl) were combined with calibration curve regression uncertainties (accuracy: typical error 5% F, <10% Cl) to yield no more than 10% error for F measurements, and 12% error for Cl measurements. Measurements where the standard deviation over ten counting cycles was greater than 20% were excluded from the dataset. The combination of those two errors (2SE plus error on calibration curve) corresponds to the positive error bar on all of our figures. The negative error bars are larger because, in addition to those two errors, we have added the conservative uncertainty on the maximum background defined by Herasil and Synthetic Forsterite measurements (Fig. 1).

Li, Be and B measurement details, along with electron microprobe methods for major element analyses, can be found in the supplementary materials.

## Results

### F, Cl, Li, Be and B variability in mantle minerals

#### *Measuring the primary F and Cl contents of mantle minerals*

The peridotite samples selected for this study are all relatively fresh rocks that display less than 20% alteration and minimal weathering features. Individual spot measurements and profiles were conducted on the least altered grains to minimize the potential disturbance of primary F and Cl contents of minerals by secondary processes. Individual measurements can be found in Table 1 in Electronic Supplementary Material. F and Cl concentration profiles (Table 3 in Electronic Supplementary Material) were measured in orthopyroxene for samples Fin1b (Fig. 2), Fin10 (Fig. 3), and J98-10 (Fig. S1), in clinopyroxene for samples

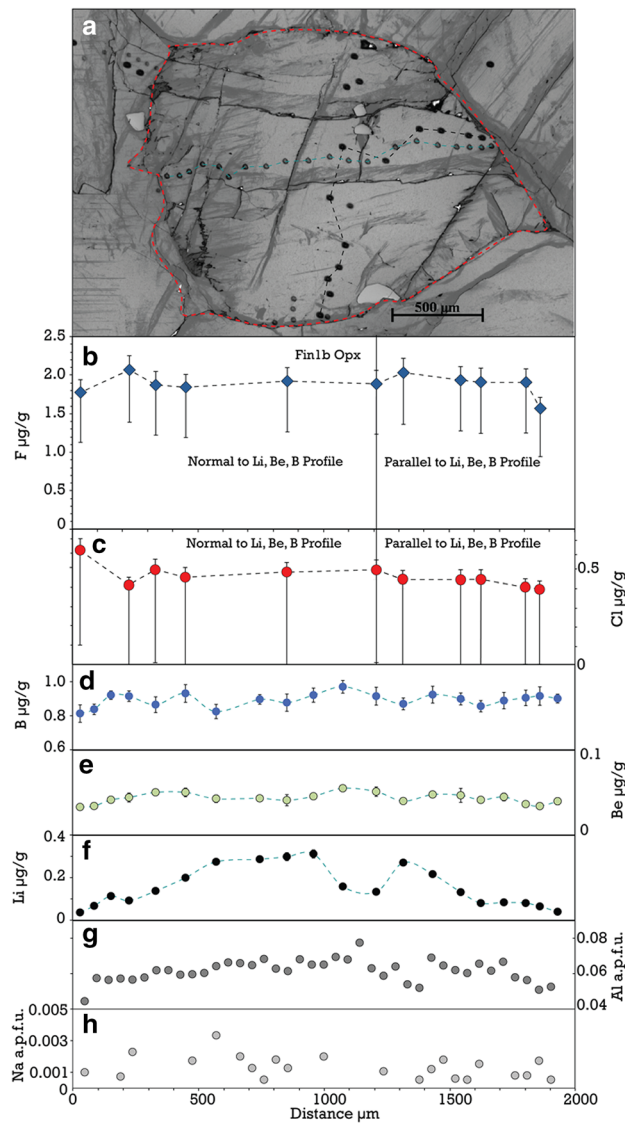


**Fig. 2** Concentration profiles in Fin1b orthopyroxene. Two F and Cl core to rim profiles were conducted, one parallel to B, Be, Li, Al, Na profiles and the other normal to it. *Positive error bars* are internal errors propagated with calibration curve errors. *Negative error bars* are internal errors propagated with calibration curve errors and maximum background errors monitored by Cl measurements in Synthetic Forsterite and F measurements in Herasil glass

Fin1b (Fig. 4), Fin10 (Fig. 5), and J127-09 (Fig. S2), and in amphibole for sample Fin1b (Fig. 6). For the Finero samples, F and Cl profiles followed the same path as Li, Be, and B profiles. Other analyses consisted of individual spots. All of our analyses were performed on surfaces devoid of cracks or other alteration features. Still, Cl concentrations showed local enrichments within the same grain, even on surfaces that appear to be pristine under reflected light (Fig. S2a). Petrographic observations using high magnification in transmitted light revealed that small fractures ( $\mu\text{m}$ -wide) located below the grain's surface and not visible in reflected

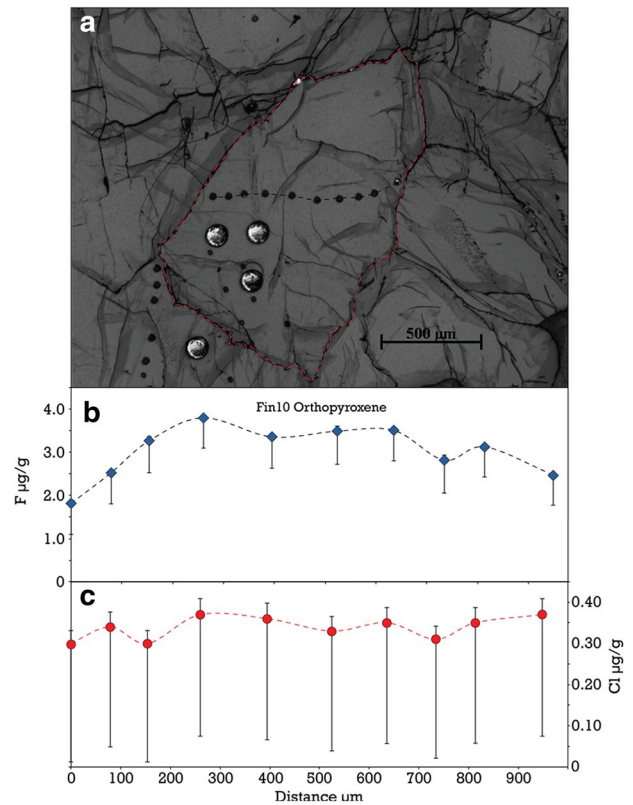


**Fig. 3** F and Cl profile across Fin10 orthopyroxene. *Positive error bars* are internal errors propagated with calibration curve errors. *Negative error bars* are internal errors propagated with calibration curve errors and maximum background errors monitored by Cl measurements in Synthetic Forsterite and F measurements in Herasil glass. Individual measurements are reported in Table 3 in Electronic Supplementary Material

light locally cause elevated Cl signals (Fig. S2c). These range from two to ten times the average Cl concentration of the grain, suggesting local Cl enrichment through secondary processes. Thus, incipient alteration can significantly affect the apparent primary Cl content of minerals. Therefore, we discarded data that were acquired within 30  $\mu\text{m}$  or less of an alteration feature present at depth ( $\sim 10\%$  of our total dataset). Fluorine concentrations were not affected by the presence of these micro-cracks (Fig. S2b).

#### *F, Cl, Li, Be and B variability along intra-grain profiles in clinopyroxene*

Apart from four high Cl values linked to the presence of micro-cracks, Cl concentrations in J127-09 clinopyroxene show limited variability across the grain (Fig. S2c). Likewise, Cl concentrations in Fin1b (Fig. 4) and Fin10 (Fig. 5) clinopyroxene are indistinguishable from core to rim. With respect to F, elevated concentrations are observed in the core of Fin1b clinopyroxene (Fig. 4). The

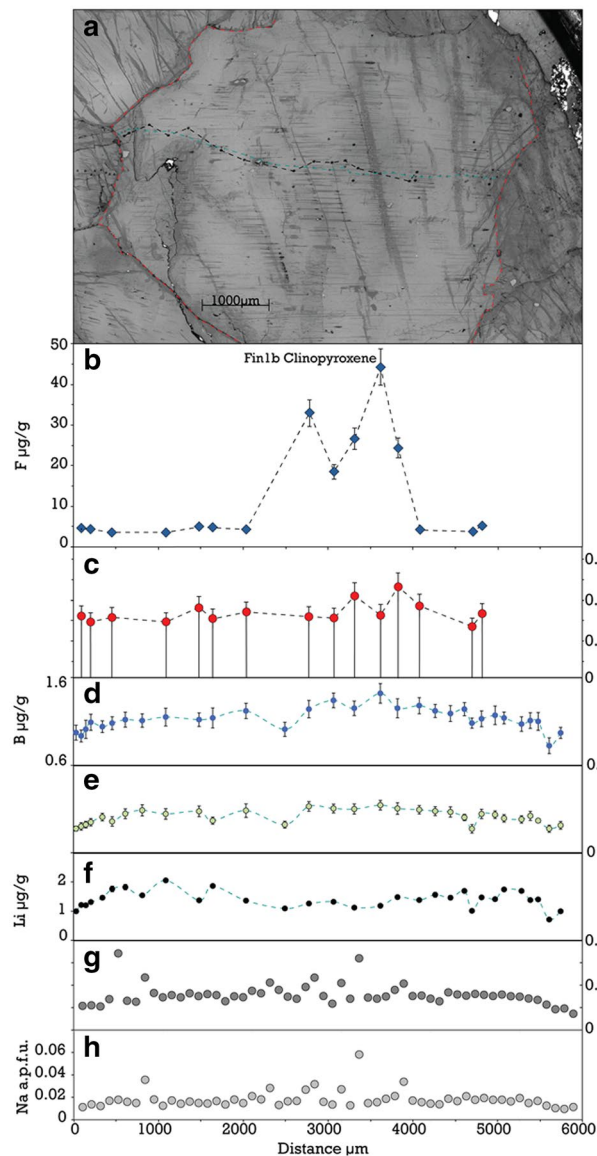


**Fig. 4** Concentration profiles for Fin1b clinopyroxene. F and Cl profiles were conducted parallel to B, Be, Li, Al, Na profiles. *Positive error bars* are internal errors propagated with calibration curve errors. *Negative error bars* are internal errors propagated with calibration curve errors and maximum background errors monitored by Cl measurements in Synthetic Forsterite and F measurements in Herasil glass. Individual measurements are reported in Tables 3 and 4 in Electronic Supplementary Material

F content of clinopyroxene can significantly vary between samples. For example, J127-09 clinopyroxene displays a restricted F content from core to rim, averaging 2.3  $\mu\text{g/g}$  (Fig. S2b). Although lower F contents are observed in the core of the grain if we only consider 2SE uncertainty, variations are indistinguishable within our conservative background values. However, in Fin10, F ranges from 18  $\mu\text{g/g}$  in the core to 6  $\mu\text{g/g}$  at the rim (Fig. 5b). In

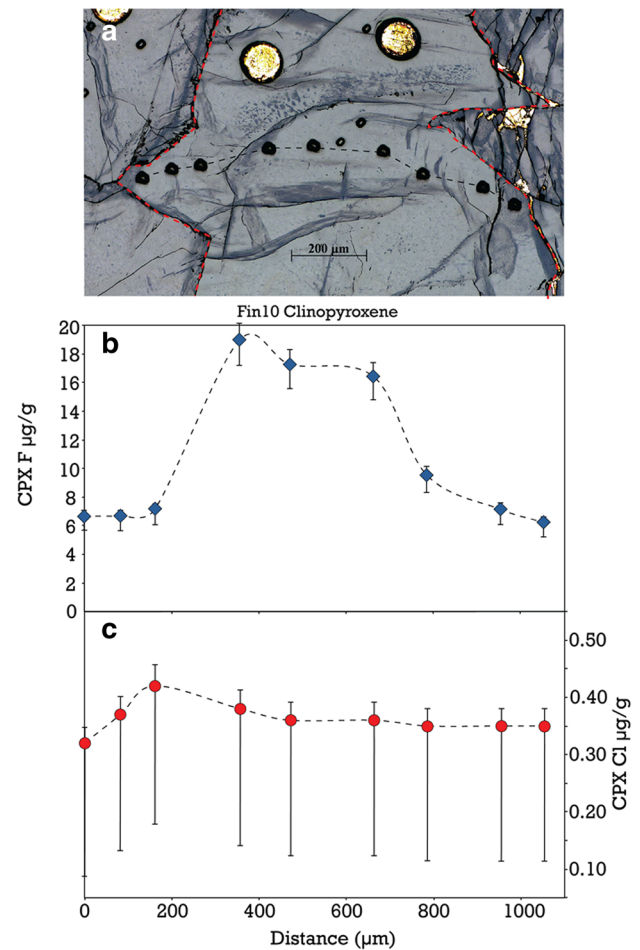


**Fig. 5** **a** Reflected light photomicrograph of Fin 10 clinopyroxene, with grain boundary outlined with red dashed line and SIMS profile denoted with black dashed line. **b** F profile and **c** Cl profile across Fin10 clinopyroxene. *Positive error bars* are internal errors propagated with calibration curve errors. *Negative error bars* are internal errors propagated with calibration curve errors and maximum background errors monitored by Cl measurements in Synthetic Forsterite and F measurements in Herasil glass. Individual measurements are reported in Table 3 in Electronic Supplementary Material

Fin1b, F is even more variable, ranging from 44  $\mu\text{g/g}$  in the core to 4  $\mu\text{g/g}$  at the rim (Fig. 4). B and Be concentrations in Fin1b are slightly higher in the core, while Li is slightly depleted in the core and directly adjacent to the rim. To summarize, the F contents of Josephine clinopyroxene are low and display limited variability, while the cores of Finero clinopyroxenes are highly enriched in F (core concentrations up to ten times the rim). In addition, profiles in Finero clinopyroxene indicate that B and Be correlate with F, while Li does not correlate with other elements.

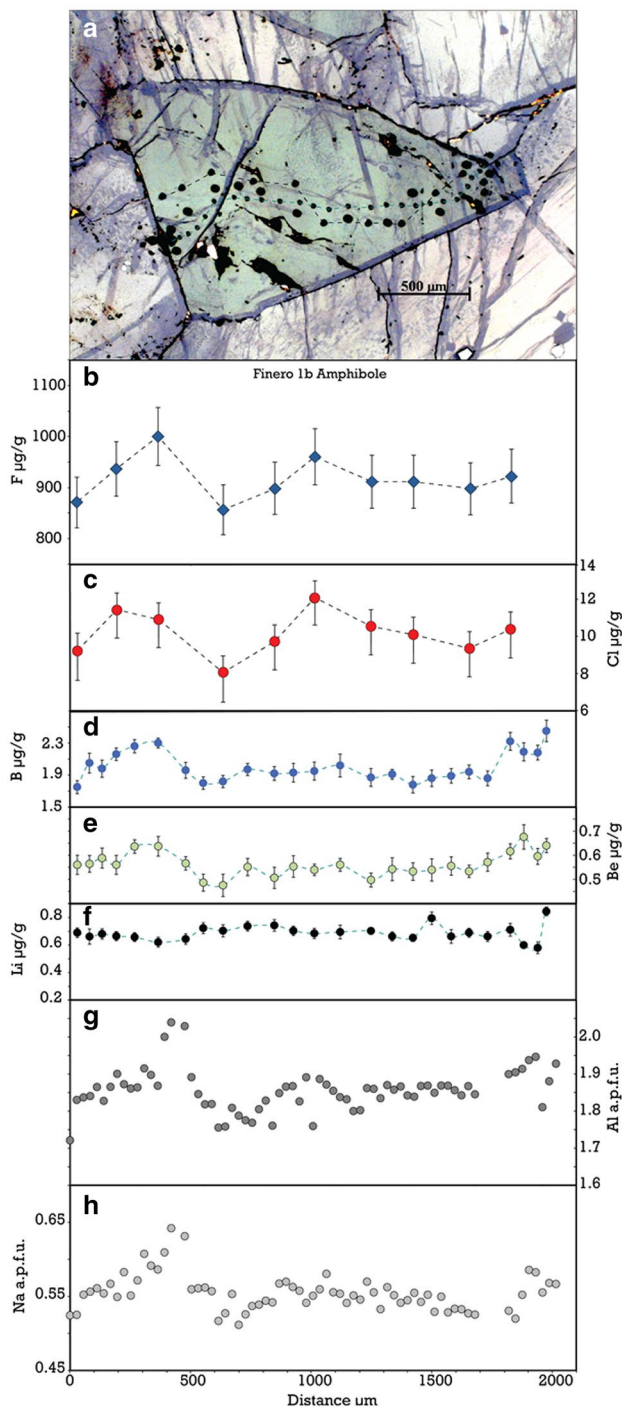


**Fig. 6** Concentration profiles in Fin1b amphibole. F and Cl profiles were conducted parallel to B, Be, Li, Al, Na profiles. *Positive error bars* are internal errors propagated with calibration curve errors. *Negative error bars* are internal errors propagated with calibration curve errors and maximum background errors monitored by Cl measurements in Synthetic Forsterite and F measurements in Herasil glass. Individual measurements are reported in Tables 3 and 4 in Electronic Supplementary Material

### *F, Cl, Li, Be and B variability along intra-grain profiles in orthopyroxene*

Cl concentrations in orthopyroxene are low and have limited variability (Figs. 2, 3, S1). Although lower F contents are observed in the core of J98-10 orthopyroxene if we only consider 2SE uncertainty (Fig. S1), we cannot distinguish variations within our conservative background values. In Fin1b orthopyroxene profile (Fig. 2), F, Be, B and Li are slightly depleted at the edges. Similar to Fin1b clinopyroxene, the core of Fin1b orthopyroxene is depleted in Li, and that depletion is not reflected in any other elements. F in Fin10 orthopyroxene is more variable (Fig. 3), ranging from 3.8 µg/g in the core to 1.8 µg/g at the rim. To summarize, the F contents of Josephine orthopyroxene are low and display limited variability, while the cores of Finero orthopyroxenes tend to be slightly enriched in F compared to the rims. Also, profiles in Finero orthopyroxene indicate that B and Be may correlate with F, but higher precision would be needed to determine this.

### *F, Cl, Li, Be and B variability along intra-grain profile in amphibole*

A hornblende amphibole from sample Fin1b was also analyzed for F, Cl, Li, Be, and B along a 2-mm profile (Fig. 6). Measurements yielded an average F and Cl content of 916 and 10.2 µg/g, respectively, significantly higher than in pyroxenes. Here, F, Cl, B and Be are clearly correlated along the grain profile. As for the pyroxenes, no clear correlation is observed between Li and the other elements.

### **Fluorine and chlorine inter-mineral partition coefficients**

Here, we evaluate the inter-mineral partition coefficients ( $D_{\text{element}}^{\text{mineral A/mineral B}}$ ) of F and Cl between orthopyroxene-clinopyroxene, olivine-orthopyroxene, and olivine-clinopyroxene (Figs. 7, 8). In Fig. 8, inter-mineral partition coefficients for Cl between olivine, orthopyroxene and clinopyroxene are near unity (between 0.94 and 1.3) within our conservative errors. Cl appears to be more compatible in clinopyroxene compared to both olivine and orthopyroxene if we only consider 2SE uncertainty; however, there are still large uncertainties on low Cl values if one considers a conservative background error. A linear inter-mineral partitioning trend for each mineral pair indicates that Cl partitioning may be controlled by similar processes in those three phases. In Fig. 7a, inter-pyroxene partitioning data from this study yield a  $D_{\text{F}}^{\text{Cpx/Opx}}$  of 2.40 with an  $r^2$  value of 0.95. In pyroxenes with low F concentrations (inset in Fig. 7b), the trend holds within error, except for one MAR analysis. A linear inter-mineral partitioning trend between

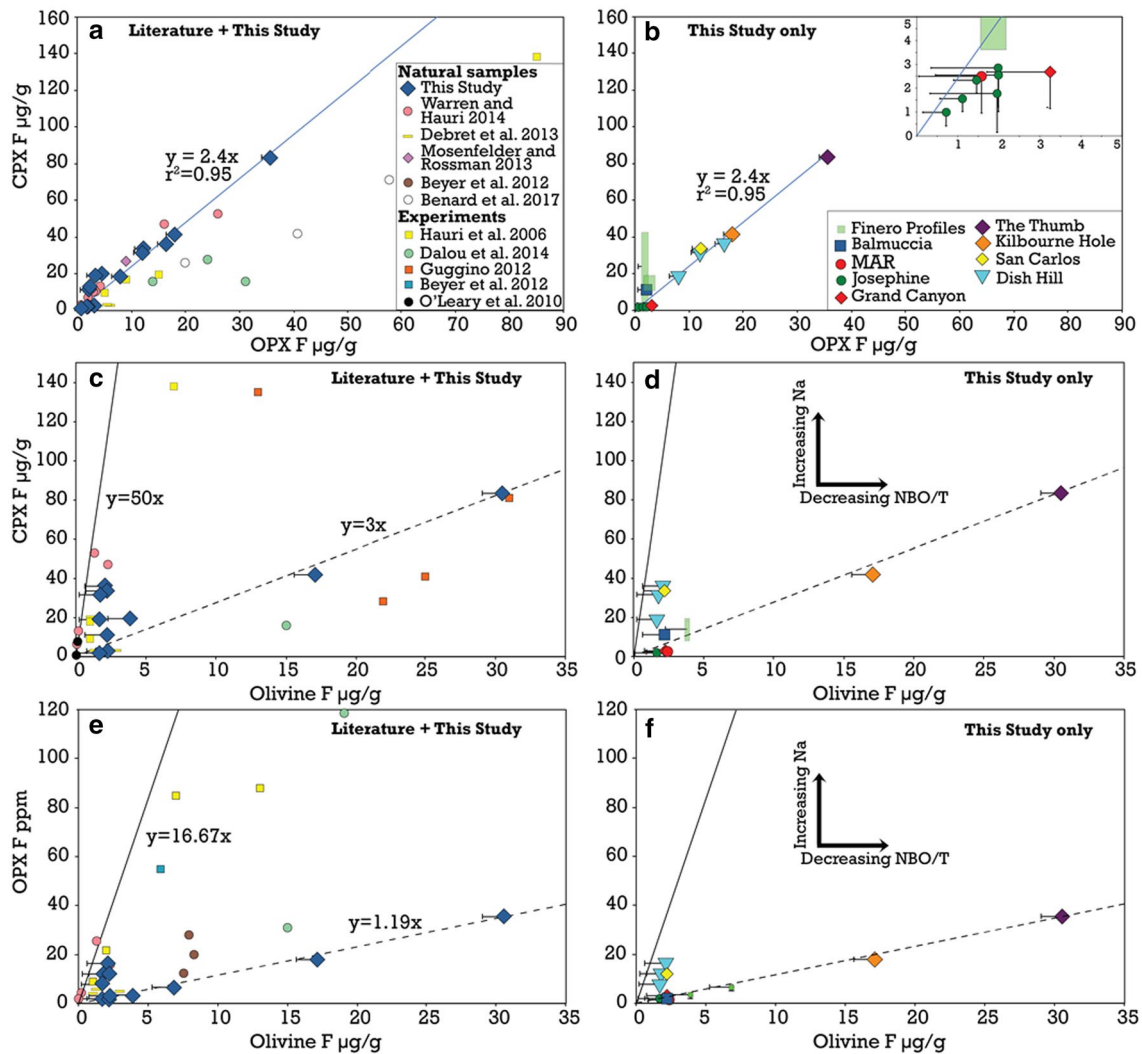


**Fig. 7** Inter-mineral partition coefficients for F between coexisting olivine, orthopyroxene and clinopyroxene. Since Finero samples have the largest intra-grain range of concentrations, profiles are identified by rectangles. **a** Opx–Cpx inter-mineral partition coefficients from the literature and this study. Blue solid line denotes linear best fit (this study only) where the slope of the line equals the inter-mineral partition coefficient. **b** Opx–Cpx inter-mineral partition coefficients from this study only. *Inset* expands low (sub-5 µg/g) F concentrations. Blue solid line denotes linear best fit (this study only) where the slope of the line equals the inter-mineral partition coefficient. **c** Ol–Cpx inter-mineral partition coefficients from the literature and this study. **d** Ol–Cpx inter-mineral partition coefficients from this study

only. **e** Ol–Opx inter-mineral partition coefficients from the literature and this study. **f** Ol–Opx inter-mineral partition coefficients from this study only. Black solid lines in **c–f** denote inter-mineral partition coefficients using data from Warren and Hauri (2014). Black dashed lines denote trends for a subset of samples from this study. Positive error bars are internal errors propagated with calibration curve errors. Negative error bars are internal errors propagated with calibration curve errors and maximum background errors monitored by CI measurements in Synthetic Forsterite and F measurements in Herasil glass. Error bars not visible are smaller than symbols. Individual measurements are reported in Table 1 in Electronic Supplementary Material

orthopyroxene and clinopyroxene indicates that F partitioning may be controlled by similar processes in pyroxenes. The trend defined by our study is also in agreement with the limited previous literature data on natural pyroxenes, but differs from experimental studies which show more scattering. In contrast, olivine-clinopyroxene (Fig. 7c, d) and olivine-orthopyroxene (Fig. 7e, f) inter-mineral partition coefficients define a wide array of values. F is systematically more compatible in clinopyroxene compared to olivine

(range of slope 3–50) and orthopyroxene (slope equal to 2.40), but F compatibility between olivine and orthopyroxene can approach unity in some samples (range of slope 1.19–16.67). Dish Hill and San Carlos samples plot near a steep trend defined by previously published values for abyssal samples (Warren and Hauri 2014). Alternatively, samples from Kilbourne Hole, Grand Canyon, the Thumb and Finero proportionally contain more F in olivine. An array of inter-mineral partitioning trends between pyroxenes and



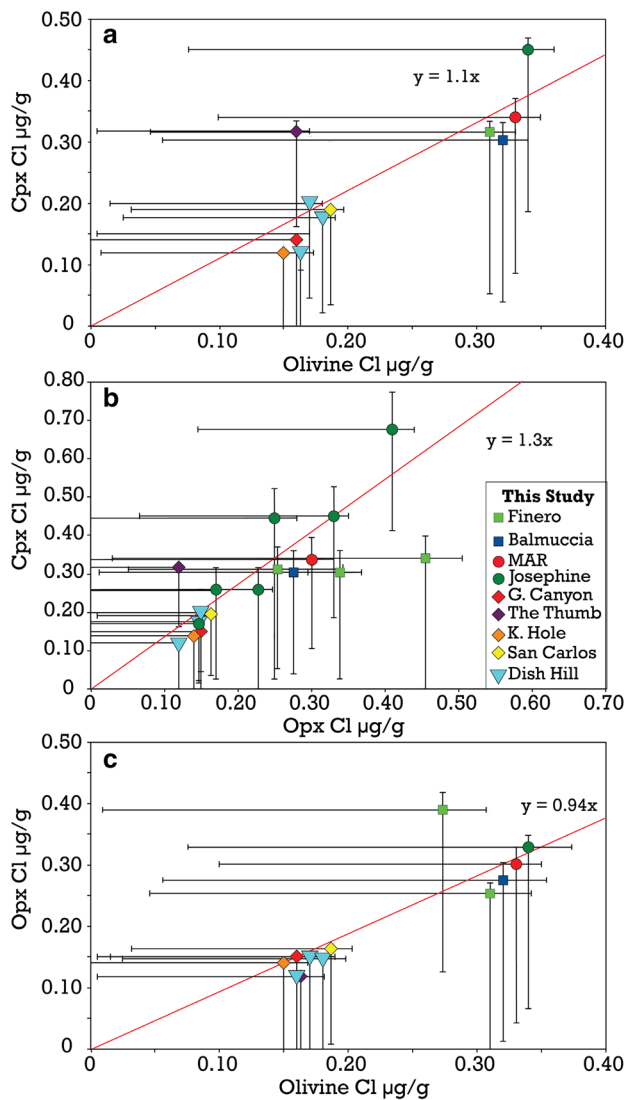


**Fig. 8** Inter-mineral partition coefficients for Cl between coexisting olivine, orthopyroxene and clinopyroxene from this study. **a** Ol–Cpx inter-mineral partition coefficients. *Red line* denotes linear best fit **b**. Opx–Cpx inter-mineral partition coefficients. *Red line* denotes linear best fit. **c**. Ol–Opx inter-mineral partition coefficients. In **a–c**, *red line* denotes linear best fit. *Positive error bars* are internal errors propagated with calibration curve errors. *Negative error bars* are internal errors propagated with calibration curve errors and maximum background errors monitored by Cl measurements in Synthetic Forsterite and F measurements in Herasil glass. Individual measurements are reported in Table 1 in Electronic Supplementary Material

olivine indicates that controls on F partitioning are different for those minerals. Based on inter-mineral partitioning data, we infer that Cl compatibility ranks as follows: amphibole > cpx > olivine ~ opx, while for F compatibility ranks as follows: amphibole > cpx > opx ≥ olivine, depending on the tectonic context of the samples. For comparison, Hauri et al. (2006) and Dalou et al. (2012) concluded that F compatibility is arranged as cpx > opx > garnet > olivine, while

Mosenfelder (Mosenfelder and Rossman 2013a) concluded that cpx > olivine > opx > garnet. Our new inter-mineral partitioning data reconcile previous discrepancies as they illustrate how orthopyroxene and olivine from different tectonic environments can accommodate variable amounts of F, leading to variable halogen compatibility as a function of mineral chemical composition, melt/fluid composition, and potentially extrinsic variables such as pressure and temperature.

### Correlation between F, Cl and major elements

Major element data for all olivine, orthopyroxene, and clinopyroxene are presented in Table 4 in Electronic Supplementary Material. Major element data for Fin1b profiles in clinopyroxene (Fig. 4), orthopyroxene (Fig. 2), and amphibole (Fig. 6) can be found in Table 5 in Electronic Supplementary Material. We plotted the major element content of mantle minerals versus F and Cl to investigate the incorporation mechanisms of F and Cl in the crystal structure of minerals. The F and Cl contents of olivine do not correlate with any major element. The F content of orthopyroxene in this study displays a robust correlation ( $r^2 = 0.95$ ) with Na (Fig. 9a, b). Although no correlation is observed between Al and F in orthopyroxene from different samples (Fig. S3b), Al content and F–Be–B in Fin1b orthopyroxene are consistently depleted at the rims (Fig. 2), which could indicate that they broadly correlate. Na is too low to show any correlation. The F content of clinopyroxene analyzed in this study also displays a broad correlation ( $r^2 = 0.84$ ) with Na (Fig. 9c, d). Although no relationship is observed between Al and F in clinopyroxene from different samples (Fig. S3a), we observe a correlation between Na and Al content and F–Be–B in Fin1b clinopyroxene, where all those elements are enriched in the core of the grain (Fig. 4). Recasting clinopyroxene chemical compositions into end-member pyroxene compositions (En, Fs, Wo) showed no relationship with F concentration, nor with  $D_F^{cpx/melt}$  beyond the negative En versus  $D_F^{cpx/melt}$  correlation shown by Guggino (2012). In addition, Na and Al clearly correlate with F–Cl–Be–B in amphibole (Fig. 6).

## Discussion

### Incorporation mechanisms of F and Cl in olivine

Major element data from this study do not correlate with F and Cl concentrations in olivine, indicating that their incorporation may not be primarily controlled by crystal chemistry. That being said, trends between major elements (wt%) and halogens (μg/g) in olivine are difficult to discern and we leave open the possibility of coupled exchanges

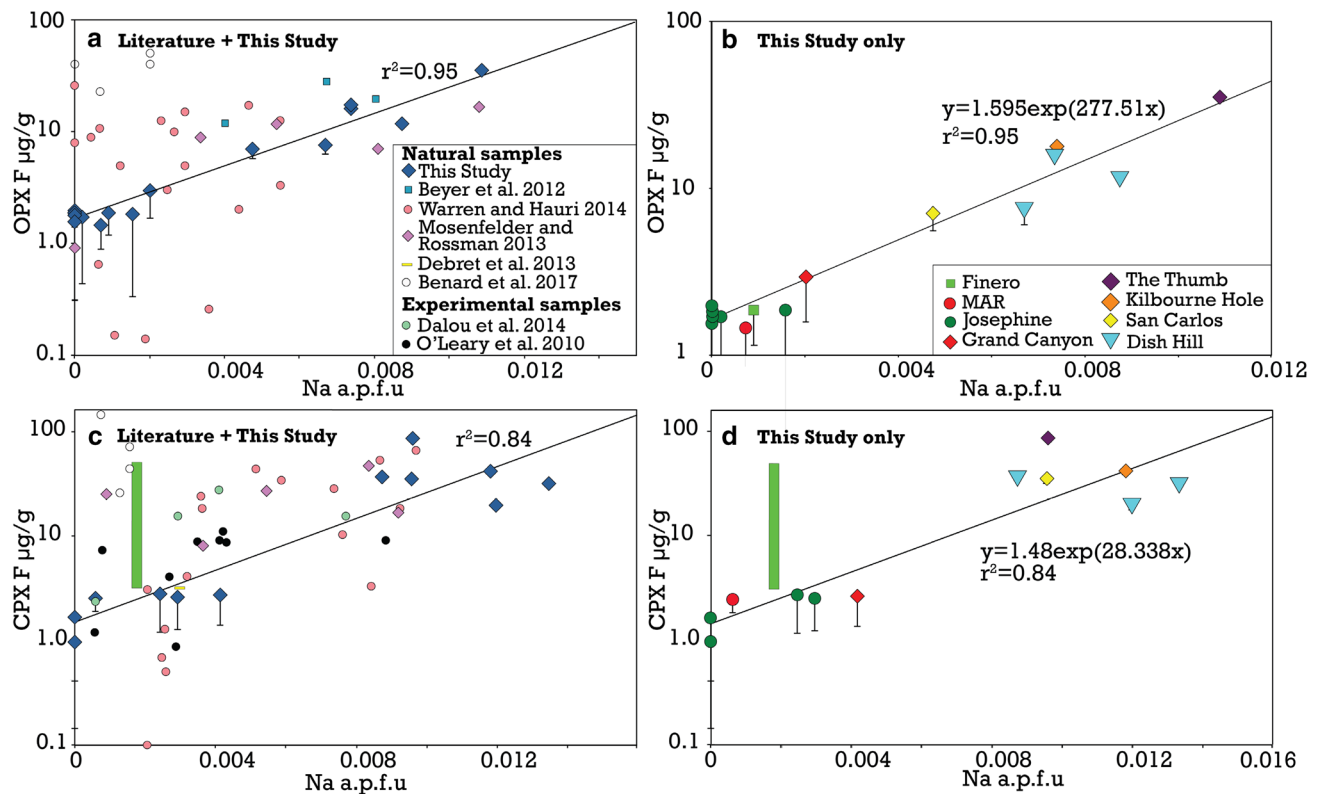


**Fig. 9** **a** Orthopyroxene Na content in atoms per formula unit (a.p.f.u) versus F  $\mu\text{g/g}$  for all available experimental and natural data, including this study. **b** Orthopyroxene Na content in a.p.f.u. versus F  $\mu\text{g/g}$  for all natural samples from this study only. **c** Clinopyroxene Na content in a.p.f.u. versus F  $\mu\text{g/g}$  for all available experimental and natural data, including this study. **d** Clinopyroxene Na content in a.p.f.u. versus F  $\mu\text{g/g}$  for all natural samples from this study only. In **a–d**, the solid black line denotes best fit. For Finero sample,

green bars show range of values along profiles. Positive error bars are internal errors propagated with calibration curve errors. Negative error bars are internal errors propagated with calibration curve errors and background errors monitored by F measurements in Herasil glass. Error bars not visible are smaller than symbols. Individual measurements are reported in Tables 2, 3 and 4 in Electronic Supplementary Material

between species at low concentrations. To our knowledge, no incorporation mechanism has been proposed for Cl in olivine, and the lack of experimental data for Cl partitioning between olivine and melt prevent us from investigating the effect of melt composition on the Cl content of olivine.

A limited number of experimental studies provide information on the partitioning of F between olivine and mantle-derived melts (Hauri et al. 2006; O'Leary et al. 2010; Beyer et al. 2012; Guggino 2012; Bernini et al. 2013; Dalou et al. 2014). Guggino (2012) suggests that F partitioning is controlled primarily by the ratio of non-bridging oxygen atoms to tetrahedrally coordinated cations (NBO/T) in the melt, where NBO/T decreases with increasing degree of polymerization in the silicate melt (Mysen and Cody 2004; Mysen 2007b). We compiled experimental studies that provide partition coefficients of F between olivine and silicate melt ( $D_F^{\text{olivine/melt}}$ ) at  $T \approx 1000\text{--}1360$  °C and  $P \approx 0.1\text{--}3$  GPa, and calculated the NBO/T of mantle-like melts in those experiments (Fig. 10). We included both hydrous and anhydrous experimental data due to limited

available data; therefore the water content of the mineral phases could be an additional variable, which cannot be addressed at present. We incorporated the depolymerizing effects of  $\text{H}_2\text{O}$  (Mysen 2007b) and F (Dalou et al. 2014) on the NBO/T values, assuming equivalent effects of  $\text{H}_2\text{O}$  and F on melt polymerization (Dalou et al. 2014). The combined  $\text{H}_2\text{O}$  and F corrections improve the fit slightly ( $r^2$  from 0.89 to 0.92). The robust positive correlation between  $D_F^{\text{olivine/melt}}$  and the degree of melt polymerization indicates that if melting or melt-rock reaction produces more polymerized melts, increasing amounts of F are accommodated in the crystal structure of olivine, as originally suggested by Guggino (2012) and confirmed by this compilation. F compatibility in olivine increases by an order of magnitude with increasing melt polymerization (Fig. 10a). Mysen (2007a) found similar melt polymerization effects on the partitioning of Ca, Mg, and transition metals between olivine and melt, where mineral-melt partition coefficients exponentially increased with melt polymerization. We note that oxygen fugacity could also play a role in the incorporation

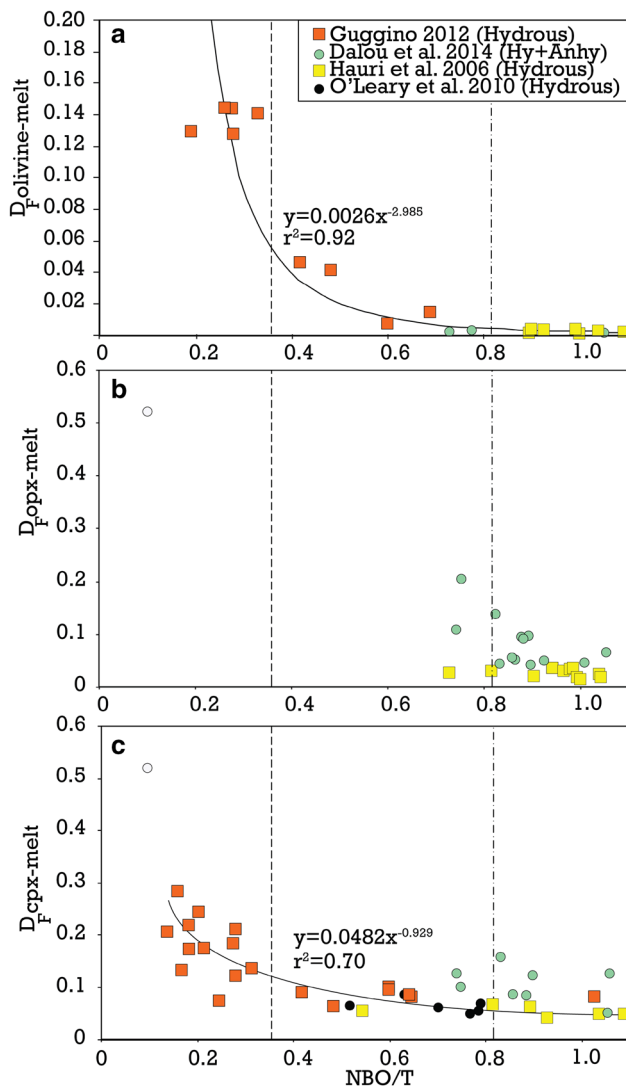


**Fig. 10** Mineral-melt partition coefficients for F plotted against NBO/T of mantle melts, corrected for the depolymerizing effects of F and H<sub>2</sub>O. **a** Olivine-melt, **b** orthopyroxene-melt, and **c** clinopyroxene-melt. Published experiments have been performed at  $T \approx 1000$ – $1360$  °C and  $P \approx 0.1$ – $3$  GPa. Vertical dashed lines represent the NBO/T for an average basaltic andesite composition from GeoRoc database (0.358), and the NBO/T for average MORB composition (0.81) from Gale et al. (2013)

of halogens into the crystal structure by charge balancing with Fe<sup>3+</sup> (Guggino 2012). However, using the calculated ferric iron content of our samples, we did not observe an obvious correlation between ferric iron and halogen content in our samples. Olivine mineral-melt partition coefficients from available literature show slight temperature dependence, however, this effect does not appear to be the dominant control on the NBO/T trend. Thus, the data indicate that the effect of melt polymerization plays a larger role than does temperature on the partitioning of F between olivine and melt.

### Incorporation mechanism of F and Cl in orthopyroxene

The F content of orthopyroxene is strongly controlled by Na content ( $r^2 = 0.95$ ; Fig. 9b). Thus, our measurements from natural samples support an incorporation mechanism where Na<sup>+</sup> in the M2 octahedral site charge balances F in the O sites. We also found that Al may correlate with FcBe–B in orthopyroxene, in agreement with Mosenfelder who suggested that Al might play a limited role in F incorporation in orthopyroxene. Experimental datasets that provide  $D_F^{\text{opx/melt}}$  and NBO/T of melts (Fig. 10b) are more limited than for clinopyroxene and olivine. However, given the strong correlation that we obtain between F and Al–Na contents in our natural orthopyroxene, crystal chemistry is likely the primary control on F incorporation into natural orthopyroxene. The variability observed in inter-mineral partitioning values of F between orthopyroxene and olivine (Fig. 7e, f) is linked to the fact that F in olivine is controlled by the NBO/T of melts, while F in orthopyroxene is primarily controlled by the Na and Al content of orthopyroxene.

### Incorporation mechanism of F and Cl in clinopyroxene

Experimental literature data for water content and fluorine content of cpx show a broad correlation ( $r^2 = 0.64$ ) that implies similar incorporation mechanisms for those two elements, e.g., tetrahedral Al<sup>3+</sup> charge balancing F. Our data, aggregated with the literature data, show a broad positive correlation between Na and F contents of clinopyroxene (Fig. 9c, d), indicates that crystal chemistry exerts influence on the incorporation of F into clinopyroxene. In Finero samples (Fig. 4), both Na and Al correlate with F–Be–B, confirming that Al should also play a role in the incorporation of F into clinopyroxene. K<sub>2</sub>O data is unavailable but it has also been suggested that coupled K<sup>+</sup> substitution in the pyroxene M sites may be another mechanism for F incorporation into clinopyroxene (Mosenfelder and Rossman 2013b). Melt composition can also play a role in halogen partitioning between clinopyroxene and melt (Dalou et al. 2012, 2014; Guggino 2012; Bénard et al. 2017). We compiled available experimental data on halogen partitioning between cpx and melt (Hauri et al. 2006; O’Leary et al. 2010; Guggino 2012; Dalou et al. 2014), in experiments performed at  $T \approx 1000$ – $1360$  °C and  $P \approx 0.1$ – $3$  GPa. We used both anhydrous and hydrous experimental data due to the limited literature data available, and corrected NBO/T for the depolymerizing effects of H<sub>2</sub>O and F as outlined in Dalou et al. (2014). We note that the water content of mineral phases could be an additional variable, which cannot be addressed with the current data. In Fig. 10c, a broad correlation exists between NBO/T of experimental melts and F concentrations in clinopyroxene where the amount of F

incorporated in clinopyroxene increases with increasing melt polymerization ( $r^2 = 0.70$ ). Similar effects have been found for trace elements in clinopyroxene, where the mineral-melt partition coefficient increases exponentially with increasing melt polymerization (Gaetani 2004). Our data, combined with previous experimental studies, support the hypothesis that there are various means by which halogens can be incorporated into the crystal lattice of clinopyroxene. We conclude that the F content of clinopyroxene is a function of both crystal chemistry (e.g., Na and Al contents) and melt structure (NBO/T). We note that oxygen fugacity, and thereby ferric iron content could also play a role in the accommodation of F in cpx, however, we did not find a correlation between ferric iron content (calculated by stoichiometry) and F concentration in our samples. Further work would be needed to better constrain the role of ferric iron in the accommodation of crystal site defects. The variability observed in inter-mineral partitioning values of F between clinopyroxene and olivine (Fig. 7c, d) is linked to the fact that F in olivine is primarily controlled by the NBO/T of melts, while F in clinopyroxene is controlled by a combination of crystal chemistry and melt structure.

### Halogens as tracers of fluid/melt percolation in mantle minerals

Samples from our study come from a variety of tectonic environments and provide valuable information on the cycling of halogens during various mantle processes.

Josephine samples have the highest Cl concentrations in clinopyroxene ( $>0.6 \mu\text{g/g}$ ) and olivine ( $>0.4 \mu\text{g/g}$ ), and one of the highest Cl concentrations in orthopyroxene ( $>0.4 \mu\text{g/g}$ ). Although those values are conservatively considered as maximum values, the most depleted samples in our study contain the highest Cl contents (Fig. 8), and the lowest F values ( $<3 \mu\text{g/g}$  F; Fig. 7). Low F contents in the Josephine samples are consistent with high degrees of flux melting in the Josephine peridotite (Le Roux et al. 2014), whereas slight enrichment in Cl and F at the edges of pyroxene grains (Figs. S1, S2) are consistent with late percolation of Cl–F–fluids/hydrous melts (e.g., boninite; Le Roux et al. 2014).

Cl concentrations in minerals from Dish Hill, Kilbourne Hole, San Carlos and Grand Canyon are the lowest of our sample selection and do not record the percolation of Cl-rich fluids. F contents in samples from Dish Hill and San Carlos plot near a steep trend defined by previously published values for abyssal samples (Fig. 7) (Warren and Hauri 2014). The fact that the Dish Hill samples follow a similar trend as abyssal peridotites is consistent with a process where Dish Hill lherzolites formed by melting and refertilization beneath mid-ocean ridges (Luffi et al. 2009). The same authors suggest that the mantle underneath Dish

Hill has been rejuvenated by the emplacement of flat-subducted young oceanic peridotites. In contrast, samples from Grand Canyon, Kilbourne Hole, and the Thumb define a distinct trend (Fig. 7c–f). Those samples contain proportionally more F in olivine, which we ascribe to increased compatibility of F in olivine during melt-rock reactions with, polymerized (siliceous) and hydrous melts. This interpretation supports the findings of Lee (2005) who postulated that the REE patterns found in Thumb xenoliths require interaction with a slab melt. This is also in agreement with previous work that showed that flat slab subduction of the Farallon plate during the early Cenozoic hydrated the subcontinental lithospheric mantle (Dixon et al. 2004; Lee 2005; Humphreys and Niu 2009), and with the fact that the Thumb minerals contains the highest water content of any Colorado Plateau xenoliths (Li et al. 2008).

Core to rim variations are nearly ubiquitous in the Finero samples analyzed. The cores of Finero clinopyroxenes are enriched in F, while Finero orthopyroxenes show no such enrichments. The correlation between major elements and volatile elements likely reflects re-equilibration with several generations of fluids/melts. Finero samples plot on a similar trend defined by Grand Canyon, Kilbourne Hole and Thumb samples (Fig. 7). Thus, similar to those samples, we attribute F enrichment in olivine to interaction of the mantle with hydrous siliceous melts. Our data are consistent with previous studies which suggest that several episodes of pervasive metasomatism occurred in Finero (Zanetti et al. 1999; Giovanardi et al. 2013), which would be reflected in the core to rim variability that we observe. In particular, Selverstone and Sharp (2011) suggested that both Cl-rich fluids and an evolved hydrous melt had percolated the Finero mantle, which would explain why those samples show various generations of Cl and F enrichments. The single amphibole measured in this study (Finero 1b) shows F to be 100× more abundant than Cl, lending support to the suggestion of Bénard et al. (2017) that amphibole crystallization effectively depletes metasomatic melts in F relative to Cl due to the compatible nature of F in amphibole. Although rapid diffusion of Li may have erased correlations between Li and other elements, a multi-phase process would also explain the depletions in F, Li, Be and B in the rims of mantle minerals. It is not clear whether Cl is enriched or depleted at the grain edges. The late percolation of fluids could have leached F, B, Be and Li out of the pyroxene grains, resulting in the rim depletions. Such rim depletions are observed in all grains, hence those elements must have been lost from the rock when a fluid phase migrated along the grain boundaries. Taken together, the F, Cl (and Li–Be–B) variations in pyroxenes and amphibole depict a multi-stage history in Finero that involves diffusive re-equilibration and interaction with several generations of fluids/melts.

Finally, F in the MAR pyroxenes and olivine does not follow the trend defined by the limited number of abyssal samples (Warren and Hauri 2014). Further work is needed to identify the reason for inter-oceanic variability. Also noteworthy, the minerals from Balmuccia (BM5) plot between the two extreme trends defined by Dish Hill and Thumb (Fig. 7c, d), showing no specific enrichment from Cl-rich fluids or F-rich hydrous melts, consistent with a mantle that experienced limited amounts of metasomatism.

### Fluorine and chlorine budget of the upper mantle

Previous studies have indirectly estimated the F–Cl budget of the MORB mantle using the halogen content of primitive basalts (Salters and Stracke 2004) and olivine-hosted melt inclusions (Saal et al. 2002). In particular, these studies have relied on elemental ratios that are minimally fractionated during mantle melting, (e.g., F/P, F/Nd, Cl/K, and Cl/P) and/or on elemental correlations (e.g., CO<sub>2</sub> vs Cl) to estimate the halogen budget of the MORB mantle. Estimates range from 11–17 µg/g F and 0.38–5 µg/g Cl for depleted MORB mantle (Saal et al. 2002; Salters and Stracke 2004; Workman and Hart 2005; Le Roux et al. 2006; Shaw et al. 2010; Beyer et al. 2012; Le Voyer et al. 2015) to 8–31 µg/g F and 0.4–22 µg/g Cl (Shimizu et al. 2016) if ultra-depleted (D-DMM) and enriched MORB mantle (E-DMM) are accounted for (Table 6 in Electronic Supplementary Material). Based on results from this study, we provide two independent methods to estimate the F and Cl budget of the upper mantle.

First, we use a compilation of published partition coefficients (Fig. 10) and inter-mineral partition coefficients from this study (Figs. 7a, b) to estimate the bulk partition coefficients for F and Cl applicable to DMM melting. Experimental literature provides highly variable data for halogen partitioning between olivine, pyroxene, and silicate melts.  $D_F^{\text{olivine/melt}}$  ranges from 0.007 to 0.146 (Hauri et al. 2006; Dalou et al. 2012; Guggino 2012; Dalou et al. 2014),  $D_F^{\text{opx/melt}}$  ranges from 0.016 to 0.139 (Hauri et al. 2006; Dalou et al. 2012, 2014), and  $D_F^{\text{cpx/melt}}$  ranges from 0.005 to 0.219 (Hauri et al. 2006; O’Leary et al. 2010; Dalou et al. 2012, 2014; Guggino 2012). To estimate the bulk partition coefficients of F and Cl during DMM melting, we use the correlation between  $D_F^{\text{olivine/melt}}$ ,  $D_F^{\text{cpx/melt}}$  and NBO/T (Fig. 10a, c) of average N-MORB (0.81; (Gale et al. 2013). For DMM melting,  $D_F^{\text{olivine/melt}} = 0.005$  and  $D_F^{\text{cpx/melt}} = 0.051$ . We then utilize the robust correlation of F in coexisting pyroxenes (slope of 2.40 in Fig. 7b), to calculate  $D_F^{\text{opx/melt}} = 0.02$ . Based on the modal abundances of DMM (Workman and Hart 2005), these calculations together yield  $D_F^{\text{mantle/melt}} = 0.017$ . Experimental data for Cl partitioning is very limited. Here we use  $D_F^{\text{opx/melt}}$  of  $0.002 \pm 0.001$  from the anhydrous experiment CD1H0

(Dalou et al. 2014) and use inter-mineral partitioning data to calculate a  $D_F^{\text{cpx/melt}} = 0.003$  based on the inter-mineral partition slope of our data of 1.3. Our data show that olivine and orthopyroxene have similar partition coefficients for Cl, thus we use the same value for olivine as orthopyroxene of 0.002. These calculations together yield  $D_F^{\text{mantle/melt}} = 0.002 \pm 0.001$ , an order of magnitude lower than the bulk partition coefficient for F. MORB contain on average  $250 \pm 50$  µg/g F and 2–400 µg/g Cl for MORB unaffected by hydrothermal alteration (Saal et al. 2002). We assume a batch melting model using the above bulk partition coefficients for F and Cl and average literature F–Cl values in MORB. This procedure yields oceanic peridotitic mantle values of  $4.3 \pm 0.9$  µg/g for F and 0.004–0.82 µg/g for Cl, which is lower than most previous studies have proposed (Table 6 in Electronic Supplementary Material) but within the range proposed by Shimizu et al. (2016) and Saal et al. (2002).

Second, we use the F and Cl contents and modal proportions of olivine, orthopyroxene and clinopyroxene from this study to estimate the F and Cl variability of anhydrous peridotite mantle, assuming that all F and Cl is contained in those three minerals and that apatite is not stable in the source of MORB (Konzett and Frost 2009). Our bulk anhydrous peridotite values (excluding hydrous samples from Ivrea Zone) define a range from 1.39 to 31.1 µg/g for F and from 0.14 to 0.38 µg/g for Cl (Table 6 in Electronic Supplementary Material). Our Cl values are in good agreement with Workman and Hart’s estimate of  $0.38 \pm 0.25$  µg/g. Samples believed to be derived from the oceanic mantle (e.g., MAR, Dish Hill) yield more restricted bulk F contents (2.1–9.4 µg/g) that are within the range of the estimate based on bulk partitioning for DMM melting (~4 µg/g), and within the lower range of previously published values (e.g.,  $11 \pm 4.5$  µg/g; (Salters and Stracke 2004). The range of F content observed in bulk anhydrous peridotite (Table 6 in Electronic Supplementary Material) strongly reflects the heterogeneous distribution of F in the Earth’s upper mantle, and indicates that F is likely enriched in the mantle wedge of subduction zones, as observed in xenoliths from the Colorado Plateau. The presence of F-rich subduction-derived components in the source of MORB could explain why bulk mantle F calculated in oceanic peridotites in this study (2.1–9.4 µg/g) is lower than bulk mantle F previously calculated from MORB (11–17 µg/g). Consistent with this hypothesis, Beyer et al. (2016) suggested that eclogitized oceanic crust could host more F (in omphacitic cpx) per mass unit than the depleted oceanic mantle which is typically cpx poor. In this case, F is transported in the down-going slab via serpentine and amphibole (often tens to thousands of µg/g F), then is partitioned into omphacite upon phase changes as the slab thermally equilibrates, dehydrates, and forms eclogite, effectively returning F to

the mantle (Van den Bleeken and Koga 2015). Later melting of such halogen-rich lithologies (cpx in particular) could then account for halogen enrichments found in ocean island basalts.

All peridotite samples, regardless of their tectonic setting, yield bulk Cl values (0.14–0.38  $\mu\text{g/g}$ ) that are lower than previously published values for DMM (0.4–5  $\mu\text{g/g}$ ; Saal et al. 2002; Shaw et al. 2010; Shimizu et al. 2016) and more restricted than our estimate of DMM based on bulk partitioning (0.004–0.82  $\mu\text{g/g}$ ) (Fig. 11). Two scenarios can explain the fact that measured bulk Cl in all mantle peridotites (olivine and pyroxenes combined) is lower than the estimated bulk Cl content of DMM. First, the presence of Cl-rich recycled components in the source of MORB could explain the discrepancy, although there are no constraints on the Cl content of recycled oceanic crust. Second, N-MORB

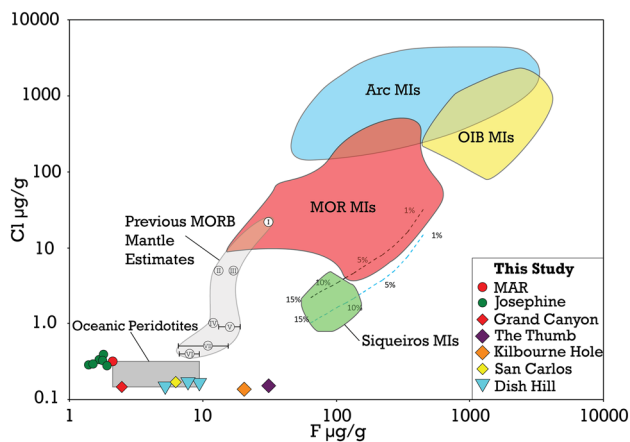


**Fig. 11** Halogen budget of the mantle as inferred from this study. Hollow circles with Roman numerals denote previous DMM estimates. Error bars shown are those provided (if any) by the literature source. (I) E-DMM, (Shimizu et al. 2016). (II) Pacific Mantle, (Shimizu et al. 2016). (III) Gakkal Ridge Mantle, (Shaw et al. 2010). (IV) DMM, (Le Voyer et al. 2015). (V) DMM, (Saal et al. 2002). (VI) D-DMM, (Shimizu et al. 2016). (VII) DMM, (Salters and Stracke 2004). Dashed box denotes DMM estimate from this study, as collected from in situ measurements of oceanic peridotites. Melting trends reflect non-modal fractional melting in the spinel stability field with calculated bulk F content of sample DHS02 (9.4  $\mu\text{g/g}$ ), and a bulk Cl content of 0.15  $\mu\text{g/g}$  (blue dashed line) and 0.32  $\mu\text{g/g}$  (black dashed line). Partition coefficients for this melting model use the NBO/T parameterization of MORB melts for F (see text) and sample CD1H0 for Cl from Dalou et al. (2014). Mantle mineral modal composition of Workman and Hart (2005). Individual measurements from this study use the same symbols as Fig. 7. Opaque fields denote olivine-hosted melt inclusion data from various tectonic settings. Siqueiros measurements (East Pacific Rise, Siqueros Transform) from Saal et al. (2002). Mid-ocean ridge MI data from various sources (Shaw et al. 2010; Wanless and Shaw 2012; Wanless et al. 2014, 2015; Le Voyer et al. 2015). Ocean island basalt MI data aggregated from the literature (Kendrick et al. 2014; Cabral et al. 2014; Rose-Koga et al. 2017). Arc olivine-hosted melt inclusion data from the literature (Portnyagin et al. 2007; Bouvier et al. 2008; Sadofsky et al. 2008; Bouvier et al. 2010; Rose-Koga et al. 2012, 2014)

is considered to be uncontaminated by seawater if their Cl/K ratio is 0.01–0.02 or less. However, Cl contamination in MORB by assimilation of hydrothermally altered rock could occur (Michael and Schilling 1989). A very minor contribution of seawater to melts (one to ten parts per thousand) can drastically alter the Cl content of the composite melt. Thus, if all MORB actually experienced some degree of Cl contamination from interaction with seawater or contamination from seawater-rich material at depth, Cl DMM estimates calculated from MORB and olivine-hosted melt inclusions could be overestimated. To illustrate this, we plotted previous MORB mantle estimates and olivine-hosted melt inclusion (MI) data from various tectonic settings (Table 7 in Electronic Supplementary Material) along with measurements from this study (Fig. 11). Interestingly, our peridotitic MORB mantle F and Cl values used to calculate the melting trends shown in Fig. 11 agree well with the primary melt inclusion data of Saal et al. (2002). This could indicate that the source of the Siqueiros MIs is composed of pure peridotite mantle, (i.e., no enriched component) and that MI Cl contamination is nil.

## Conclusion

We have developed a technique to reliably measure the F and Cl contents of natural peridotite minerals by SIMS down to  $\geq 0.4 \mu\text{g/g}$  F and  $\geq 0.3 \mu\text{g/g}$  Cl. This work is the first extensive study of the distribution of F and Cl in coexisting natural peridotite minerals (olivine, orthopyroxene, clinopyroxene, and amphibole). Halogen intra-grain variation can be significant, and the utilization of profiles as opposed to single spots when measuring grains is important to properly characterize minerals. Using previously published experimental studies, we argue that the F content of olivine is strongly controlled by NBO/T of silicate melts, which reflects melt polymerization, and we provide mineral/melt partition coefficients for F and Cl applicable to mantle melting. We propose that the F content of orthopyroxene is strongly controlled by Na and Al content. In addition, the F (and potentially Cl) content of clinopyroxene is controlled by a combination of crystal chemistry (Al, Na) and melt polymerization. In amphibole, F and Cl also correlate with major elements Al and Na. Finally, we show that F, Cl, Be and B concentrations along grain profiles are correlated in both pyroxenes and amphibole. Using F and Cl inter-mineral partition coefficients determined in this study, we show that F and Cl distribution between olivine and pyroxenes in oceanic peridotites and subduction-related peridotites is drastically different. F in oceanic peridotites is mostly hosted in pyroxenes, while the F content of olivine significantly increases in subduction-related peridotites. Further, olivine and pyroxenes from the

mantle wedge can be significantly enriched in F compared to un-metasomatized mantle, while Cl contents are consistently low ( $<1 \mu\text{g/g}$ ) in all tectonic environments. Finally, assuming that F and Cl in the anhydrous peridotite mantle is entirely contained in olivine and pyroxenes, the bulk F and Cl content of oceanic mantle ( $2.1\text{--}9.4 \mu\text{g/g}$  F;  $0.15\text{--}0.32 \mu\text{g/g}$  Cl) is lower than previous estimates for DMM. These results support the hypothesis that the source of MORB contains F-rich recycled oceanic crust. The bulk Cl budget of all anhydrous peridotites analyzed in this study ( $0.14\text{--}0.38 \mu\text{g/g}$  Cl) is lower than most previous estimates for DMM. These results suggest that virtually all MORB, including many olivine-hosted melt inclusions, could be variably contaminated by seawater-rich material at depth and that the Cl content of DMM could be overestimated. The halogen contents of mantle minerals are a unique tool to understand the distribution and cycling of halogens, from ridge settings to subduction zones.

**Acknowledgements** This research was supported by Grant NSF EAR-P&G 1524311 and DOEI Award 18563 to VLR. We thank two anonymous reviewers for their insights, which improved the manuscript. We also thank Erik Hauri for providing the Herasil glasses, Henry Dick for providing the MAR sample, and Nobumichi Shimizu for providing the Synthetic Forsterite grains. Urann was supported by the Stanley W. Watson Student Fellowship Fund based at WHOI.

## References

- Bénard A, Koga KT, Shimizu N et al (2017) Chlorine and fluorine partition coefficients and abundances in sub-arc mantle xenoliths (Kamchatka, Russia): implications for melt generation and volatile recycling processes in subduction zones. *Geochim Cosmochim Acta* 199:324–350. doi:[10.1016/j.gca.2016.10.035](https://doi.org/10.1016/j.gca.2016.10.035)
- Bernini D, Wiedenbeck M, Dolejš D, Keppler H (2013) Partitioning of halogens between mantle minerals and aqueous fluids: implications for the fluid flow regime in subduction zones. *Contrib Mineral Petrol* 165:117–128. doi:[10.1007/s00410-012-0799-4](https://doi.org/10.1007/s00410-012-0799-4)
- Beyer C, Klemme S, Wiedenbeck M et al (2012) Fluorine in nominally fluorine-free mantle minerals: experimental partitioning of F between olivine, orthopyroxene and silicate melts with implications for magmatic processes. *Earth Planet Sci Lett* 337:338:1–9. doi:[10.1016/j.epsl.2012.05.003](https://doi.org/10.1016/j.epsl.2012.05.003)
- Beyer C, Klemme S, Grützner T et al (2016) Fluorine partitioning between eclogitic garnet, clinopyroxene, and melt at upper mantle conditions. *Chem Geol* 437:88–97. doi:[10.1016/j.chemgeo.2016.05.032](https://doi.org/10.1016/j.chemgeo.2016.05.032)
- Bonifacie M, Busigny V, Mével C et al (2008) Chlorine isotopic composition in seafloor serpentinites and high-pressure metaperidotites. Insights into oceanic serpentinization and subduction processes. *Geochim Cosmochim Acta* 72:126–139. doi:[10.1016/j.gca.2007.10.010](https://doi.org/10.1016/j.gca.2007.10.010)
- Bouvier AS, Métrich N, Deloule E (2008) Slab-derived fluids in the magma sources of St. Vincent (Lesser Antilles Arc): volatile and light element imprints. *J Petrol* 49:1427–1448
- Bouvier AS, Deloule E, Métrich N (2010) Fluid inputs to magma sources of St. Vincent and Grenada (Lesser Antilles): new insights from trace elements in olivine-hosted melt inclusions. *J Petrol* 51:1597–1615
- Brenan J (1994) Role of aqueous fluids in slab to mantle transfer of B, Be, Li during subduction. *Chem Geol* 110:195–210
- Bromiley DW, Kohn SC (2007) Comparisons between fluoride and hydroxide incorporation in nominally anhydrous and fluorine-free mantle minerals. *Geochim Cosmochim Acta* 71:3570–3580
- Cabral RA, Jackson MG, Koga KT et al (2014) Volatile cycling of H<sub>2</sub>O, CO<sub>2</sub>, F, and Cl in the HIMU mantle: a new window provided by melt inclusions from oceanic hot spot lavas at Mangaia, Cook Islands. *Geochem Geophys Geosyst* 15:4445–4467. doi:[10.1002/2014GC005473](https://doi.org/10.1002/2014GC005473)
- Dalou C, Mysen BO (2015) The effect of H<sub>2</sub>O on F and Cl solubility and solution mechanisms of in aluminosilicate melts at high pressure and high temperature. *Am Miner* 100:633–643. doi:[10.2138/am-2015-4814](https://doi.org/10.2138/am-2015-4814)
- Dalou C, Koga KT, Shimizu N et al (2012) Experimental determination of F and Cl partitioning between lherzolite and basaltic melt. *Contrib Mineral Petrol* 163:591–609. doi:[10.1007/s00410-011-0688-2](https://doi.org/10.1007/s00410-011-0688-2)
- Dalou C, Koga KT, Le-Voyer M, Shimizu N (2014) Contrasting partition behavior of F and Cl during hydrous mantle melting: implications for Cl/F signature in arc magmas. *Prog Earth Planet Sci*. doi:[10.1186/s40645-014-0026-1](https://doi.org/10.1186/s40645-014-0026-1)
- Debret B, Koga KT, Nicollet C et al (2013) F, Cl and S input via serpentinite in subduction zones: implications for the nature of the fluid released at depth. *Terra Nova* 26:96–101. doi:[10.1111/ter.12074](https://doi.org/10.1111/ter.12074)
- Dingwell DB (1989) Effect of fluorine on the viscosity of diopside liquid. *Am Mineral* 3–4:333–338
- Dixon JE, Dixon TH, Bell DR, Malservisi R (2004) Lateral variation in upper mantle viscosity: role of water. *Earth Planet Sci Lett* 222:451–467. doi:[10.1016/j.epsl.2004.03.022](https://doi.org/10.1016/j.epsl.2004.03.022)
- Fabrizio A, Stalder R, Hametner K et al (2013) Experimental partitioning of halogens and other trace elements between olivine, pyroxenes, amphibole and aqueous fluid at 2 GPa and 900–1,300°C. *Contrib Mineral Petrol* 166:639–653. doi:[10.1007/s00410-013-0902-5](https://doi.org/10.1007/s00410-013-0902-5)
- Gaetani GA (2004) The influence of melt structure on trace element partitioning near the peridotite solidus. *Contrib Mineral Petrol* 147:511–527. doi:[10.1007/s00410-004-0575-1](https://doi.org/10.1007/s00410-004-0575-1)
- Gale A, Dalton CA, Langmuir CH et al (2013) The mean composition of ocean ridge basalts. *Geochem Geophys Geosyst* 14:489–518. doi:[10.1029/2012GC004334](https://doi.org/10.1029/2012GC004334)
- Giovanardi T, Morishita T, Zanetti A et al (2013) Igneous sapphirine as a product of melt-peridotite interactions in the Finero Phlogopite-Peridotite Massif, Western Italian Alps. *Eur J Mineral* 25:17–31. doi:[10.1127/0935-1221/2013/0025-2251](https://doi.org/10.1127/0935-1221/2013/0025-2251)
- Guggino SN (2012) Fluorine partitioning between nominally anhydrous minerals (olivine, clinopyroxene, and plagioclase) and silicate melt using secondary ion mass spectrometry and newly synthesized basaltic fluorine microanalytical glass standards. Arizona State University, Tempe
- Guggino SN, Hervig RL (2012) Fluorine partitioning between nominally anhydrous minerals (cpx, ol, plag) and silicate melt. In: AGU fall meeting abstracts
- Hauri E, Wang J, Dixon JE et al (2002) SIMS analysis of volatiles in silicate glasses. *Chem Geol* 183:99–114. doi:[10.1016/S0009-2541\(01\)00375-8](https://doi.org/10.1016/S0009-2541(01)00375-8)
- Hauri E, Gaetani G, Green T (2006) Partitioning of water during melting of the Earth's upper mantle at H<sub>2</sub>O-undersaturated conditions. *Earth Planet Sci Lett* 248:715–734. doi:[10.1016/j.epsl.2006.06.014](https://doi.org/10.1016/j.epsl.2006.06.014)
- Humphreys ER, Niu Y (2009) On the composition of ocean island basalts (OIB): the effects of lithospheric thickness variation and mantle metasomatism. *Lithos* 112:118–136. doi:[10.1016/j.lithos.2009.04.038](https://doi.org/10.1016/j.lithos.2009.04.038)

- Jenner FE, O'Neill HSC (2012) Analysis of 60 elements in 616 ocean floor basaltic glasses. *Geochim Geophys Geosyst*. doi:[10.1029/2011GC004009](https://doi.org/10.1029/2011GC004009)
- John T, Scambelluri M, Frische M et al (2011) Dehydration of subducting serpentinite: implications for halogen mobility in subduction zones and the deep halogen cycle. *Earth Planet Sci Lett* 308:65–76. doi:[10.1016/j.epsl.2011.05.038](https://doi.org/10.1016/j.epsl.2011.05.038)
- Kendrick MA, Jackson MG, Kent AJR et al (2014) Contrasting behaviours of CO<sub>2</sub>, S, H<sub>2</sub>O and halogens (F, Cl, Br, and I) in enriched-mantle melts from Pitcairn and Society seamounts. *Chem Geol* 370:69–81. doi:[10.1016/j.chemgeo.2014.01.019](https://doi.org/10.1016/j.chemgeo.2014.01.019)
- Konzett J, Frost DJ (2009) The high P-T stability of hydroxyl-apatite in natural and simplified MORB—an experimental study to 15 GPa with Implications for transport and storage of phosphorus and halogens in subduction zones. *J Petrol* 50:2043–2062. doi:[10.1093/ptrology/egp068](https://doi.org/10.1093/ptrology/egp068)
- Le Roux P, Shirey S, Hauri E et al (2006) The effects of variable sources, processes and contaminants on the composition of northern EPR MORB (8–10°N and 12–14°N): evidence from volatiles (H<sub>2</sub>O, CO<sub>2</sub>, S) and halogens (F, Cl). *Earth Planet Sci Lett* 251:209–231. doi:[10.1016/j.epsl.2006.09.012](https://doi.org/10.1016/j.epsl.2006.09.012)
- Le Roux V, Dick HJB, Shimizu N (2014) Tracking flux melting and melt percolation in supra-subduction peridotites (Josephine ophiolite, USA). *Contrib Mineral Petrol* 168:1064. doi:[10.1007/s00410-014-1064-9](https://doi.org/10.1007/s00410-014-1064-9)
- Le Voyer M, Rose-Koga EF, Shimizu N et al (2010) Two contrasting H<sub>2</sub>O-rich components in primary melt inclusions from Mount Shasta. *J Petrol* 51:1571–1595. doi:[10.1093/ptrology/egq030](https://doi.org/10.1093/ptrology/egq030)
- Le Voyer M, Cottrell E, Kelley KA et al (2015) The effect of primary versus secondary processes on the volatile content of MORB glasses: an example from the equatorial Mid-Atlantic Ridge (5°N–3°S). *Journal of Geophysical Research: Solid Earth* 120:125–144. doi:[10.1002/2014JB011160](https://doi.org/10.1002/2014JB011160)
- Lee CTA (2005) Trace element evidence for hydrous metasomatism at the base of the North American lithosphere and possible association with Laramide low-angle subduction. *J Geol* 113:673–685. doi:[10.1086/449327](https://doi.org/10.1086/449327)
- Li Z-XA, Lee C-TA, Peslier AH et al (2008) Water contents in mantle xenoliths from the Colorado Plateau and vicinity: implications for the mantle rheology and hydration-induced thinning of continental lithosphere. *J Geophys Res* 113:B09210–B09222. doi:[10.1029/2007JB005540](https://doi.org/10.1029/2007JB005540)
- Luffi P, Saleeby JB, Lee C-TA, Ducea MN (2009) Lithospheric mantle duplex beneath the central Mojave Desert revealed by xenoliths from Dish Hill, California. *J Geophys Res Solid Earth* 114:B03202. doi:[10.1029/2008JB005906](https://doi.org/10.1029/2008JB005906)
- Marschall HR, Altherr R, Gmüling K, Kasztovszky Z (2009) Lithium, boron and chlorine as tracers for metasomatism in high-pressure metamorphic rocks: a case study from Syros (Greece). *Miner Petrol* 95:291–302. doi:[10.1007/s00710-008-0032-3](https://doi.org/10.1007/s00710-008-0032-3)
- Michael PJ, Schilling JG (1989) Chlorine in mid-ocean ridge magmas: evidence for assimilation of seawater-influenced components. *Geochim Cosmochim Acta* 53:3131–3143. doi:[10.1016/0016-7037\(89\)90094-X](https://doi.org/10.1016/0016-7037(89)90094-X)
- Mosenfelder JL, Rossman GR (2013a) Analysis of hydrogen and fluorine in pyroxenes: I. Orthopyroxene. *Am Mineral* 98:1026–1041. doi:[10.2138/am.2013.4291](https://doi.org/10.2138/am.2013.4291)
- Mosenfelder JL, Rossman GR (2013b) Analysis of hydrogen and fluorine in pyroxenes: II. Clinopyroxene. *Am Mineral* 98:1042–1054. doi:[10.2138/am.2013.4413](https://doi.org/10.2138/am.2013.4413)
- Mysen B (2007a) Partitioning of calcium, magnesium, and transition metals between olivine and melt governed by the structure of the silicate melt at ambient pressure. *Am Mineral* 92:844–862. doi:[10.2138/am.2007.2260](https://doi.org/10.2138/am.2007.2260)
- Mysen BO (2007b) The solution behavior of H<sub>2</sub>O in peralkaline aluminosilicate melts at high pressure with implications for properties of hydrous melts. *Geochim Cosmochim Acta* 71:1820–1834. doi:[10.1016/j.gca.2007.01.007](https://doi.org/10.1016/j.gca.2007.01.007)
- Mysen BO, Cody GD (2004) Solubility and solution mechanism of H<sub>2</sub>O in alkali silicate melts and glasses at high pressure and temperature. *Geochim Cosmochim Acta* 68:5113–5126. doi:[10.1016/j.gca.2004.07.021](https://doi.org/10.1016/j.gca.2004.07.021)
- O'Leary JA, Gaetani GA, Hauri EH (2010) The effect of tetrahedral Al<sup>3+</sup> on the partitioning of water between clinopyroxene and silicate melt. *Earth Planet Sci Lett* 297:111–120. doi:[10.1016/j.epsl.2010.06.011](https://doi.org/10.1016/j.epsl.2010.06.011)
- Peslier A, Luhr J (2006) Hydrogen loss from olivines in mantle xenoliths from Simcoe (USA) and Mexico: mafic alkalic magma ascent rates and water budget of the sub-continental lithosphere. *Earth Planet Sci Lett* 242:302–319. doi:[10.1016/j.epsl.2005.12.019](https://doi.org/10.1016/j.epsl.2005.12.019)
- Philippot P, Agrinier P, Scambelluri M (1998) Chlorine cycling during subduction of altered oceanic crust. *Earth Planet Sci Lett* 161:33–44. doi:[10.1016/S0012-821X\(98\)00134-4](https://doi.org/10.1016/S0012-821X(98)00134-4)
- Portnyagin M, Hoernle K, Plechov P et al (2007) Constraints on mantle melting and composition and nature of slab components in volcanic arcs from volatiles (H<sub>2</sub>O, S, Cl, F) and trace elements in melt inclusions from the Kamchatka Arc. *Earth Planet Sci Lett* 255:53–69. doi:[10.1016/j.epsl.2006.12.005](https://doi.org/10.1016/j.epsl.2006.12.005)
- Roden MF (1981) Origin of coexisting minette and ultramafic breccia, Navajo volcanic field. *Contrib Mineral Petrol* 77:195–206. doi:[10.1007/BF00636523](https://doi.org/10.1007/BF00636523)
- Rose-Koga EF, Shimizu N, Devidal J, et al (2008) Investigation of F, S, and Cl standards by ion probe and electron microprobe. In: AGU fall meeting abstracts
- Rose-Koga EF, Koga KT, Schiano P et al (2012) Mantle source heterogeneity for South Tyrrhenian magmas revealed by Pb isotopes and halogen contents of olivine-hosted melt inclusions. *Chem Geol* 334:266–279
- Rose-Koga EF, Koga KT, Hamada M et al (2014) Volatile (F and Cl) concentrations in Iwate olivine-hosted melt inclusions indicating low-temperature subduction. *Earth Planets Space* 66:1–12. doi:[10.1186/1880-5981-66-81](https://doi.org/10.1186/1880-5981-66-81)
- Rose-Koga EF, Koga KT, Moreira M et al (2017) Geochemical systematics of Pb isotopes, fluorine, and sulfur in melt inclusions from São Miguel, Azores. *Chem Geol* 239:138–155
- Saal AE, Hauri EH, Langmuir CH, Perfit MR (2002) Vapour undersaturation in primitive mid-ocean-ridge basalt and the volatile content of Earth's upper mantle. *Nature* 419:451–455. doi:[10.1038/nature01073](https://doi.org/10.1038/nature01073)
- Sadofsky SJ, Portnyagin M, Hoernle K, van den Bogaard P (2008) Subduction cycling of volatiles and trace elements through the Central American volcanic arc: evidence from melt inclusions. *Contrib Mineral Petrol* 155:433–456. doi:[10.1007/s00410-007-0251-3](https://doi.org/10.1007/s00410-007-0251-3)
- Salters VJM, Stracke A (2004) Composition of the depleted mantle. *Geochim Geophys Geosyst*. doi:[10.1029/2003GC000597](https://doi.org/10.1029/2003GC000597)
- Scambelluri M, Müntener O, Ottolini L et al (2004) The fate of B, Cl and Li in the subducted oceanic mantle and in the antigorite breakdown fluids. *Earth Planet Sci Lett* 222:217–234. doi:[10.1016/j.epsl.2004.02.012](https://doi.org/10.1016/j.epsl.2004.02.012)
- Selverstone J, Sharp ZD (2011) Chlorine isotope evidence for multi-component mantle metasomatism in the Ivrea Zone. *Earth Planet Sci Lett* 310:429–440. doi:[10.1016/j.epsl.2011.08.034](https://doi.org/10.1016/j.epsl.2011.08.034)
- Shaw AM, Behn MD, Humphris SE et al (2010) Deep pooling of low degree melts and volatile fluxes at the 85°E segment of the Gakkel Ridge: evidence from olivine-hosted melt inclusions and glasses. *Earth Planet Sci Lett* 289:311–322. doi:[10.1016/j.epsl.2009.11.018](https://doi.org/10.1016/j.epsl.2009.11.018)
- Shimizu K, Saal AE, Myers CE et al (2016) Two-component mantle melting-mixing model for the generation of mid-ocean ridge basalts: implications for the volatile content of the Pacific upper



- mantle. *Geochim Cosmochim Acta* 176:44–80. doi:[10.1016/j.gca.2015.10.033](https://doi.org/10.1016/j.gca.2015.10.033)
- Silant'ev SA, Bortnikov NS, Shatagin KN et al (2016) Petrogenetic conditions at 18°–20°N MAR: interaction between hydrothermal and magmatic systems. *Petrology* 24:336–366. doi:[10.1134/S0869591116040044](https://doi.org/10.1134/S0869591116040044)
- Smith DK, Schouten H, Dick HJB et al (2014) Development and evolution of detachment faulting along 50 km of the Mid-Atlantic Ridge near 16.5°N. *Geochem Geophys Geosyst* 15:4692–4711. doi:[10.1002/2014GC005563](https://doi.org/10.1002/2014GC005563)
- Spilliaert N, Métrich N, Allard P (2006) S–Cl–F degassing pattern of water-rich alkali basalt: modelling and relationship with eruption styles on Mount Etna volcano. *Earth Planet Sci Lett* 248:772–786. doi:[10.1016/j.epsl.2006.06.031](https://doi.org/10.1016/j.epsl.2006.06.031)
- Straub SM, Layne GD (2003) The systematics of chlorine, fluorine, and water in Izu arc front volcanic rocks: implications for volatile recycling in subduction zones. *Geochim Cosmochim Acta* 67:4179–4203. doi:[10.1016/S0016-7037\(03\)00307-7](https://doi.org/10.1016/S0016-7037(03)00307-7)
- Van den Bleeken G, Koga KT (2015) Experimentally determined distribution of fluorine and chlorine upon hydrous slab melting, and implications for F–Cl cycling through subduction zones. *Geochim Cosmochim Acta* 171:353–373. doi:[10.1016/j.gca.2015.09.030](https://doi.org/10.1016/j.gca.2015.09.030)
- Wanless VD, Shaw AM (2012) Lower crustal crystallization and melt evolution at mid-ocean ridges. *Nat Geosci* 5:651–655. doi:[10.1038/ngeo1552](https://doi.org/10.1038/ngeo1552)
- Wanless VD, Behn MD, Shaw AM, Plank T (2014) Variations in melting dynamics and mantle compositions along the Eastern Volcanic Zone of the Gakkel Ridge: insights from olivine-hosted melt inclusions. *Contrib Mineral Petrol* 167:1005. doi:[10.1007/s00410-014-1005-7](https://doi.org/10.1007/s00410-014-1005-7)
- Wanless VD, Shaw AM, Behn MD et al (2015) Magmatic plumbing at Lucky Strike volcano based on olivine-hosted melt inclusion compositions. *Geochem Geophys Geosyst* 16:126–147. doi:[10.1002/2014GC005517](https://doi.org/10.1002/2014GC005517)
- Warren JM, Hauri EH (2014) Pyroxenes as tracers of mantle water variations. *J Geophys Res Solid Earth* 119:1851–1881. doi:[10.1002/2013JB010328](https://doi.org/10.1002/2013JB010328)
- Workman RK, Hart SR (2005) Major and trace element composition of the depleted MORB mantle (DMM). *Earth Planet Sci Lett* 231:53–72. doi:[10.1016/j.epsl.2004.12.005](https://doi.org/10.1016/j.epsl.2004.12.005)
- Wu J, Koga KT (2013) Fluorine partitioning between hydrous minerals and aqueous fluid at 1GPa and 770–947°C: a new constraint on slab flux. *Geochim Cosmochim Acta* 119:77–92. doi:[10.1016/j.gca.2013.05.025](https://doi.org/10.1016/j.gca.2013.05.025)
- Zanetti A, Mazzucchelli M, Rivalenti G, Vannucci R (1999) The Finero phlogopite-peridotite massif: an example of subduction-related metasomatism. *Contrib Mineral Petrol* 134:107–122. doi:[10.1007/s004100050472](https://doi.org/10.1007/s004100050472)